ARTICLE

Towards practical cells: Combined use of titanium black as cathode additive and sparingly solvating electrolyte for high-energy-density lithium–sulfur batteries

Jiali Liu,[†,a] Shanglin Li, [†,b] Mayeesha Marium,[b] Binshen Wang,[b] Kazuhide Ueno,[b] Kaoru Dokko,[b] and Masayoshi Watanabe*,[a]

The lithium–sulfur (Li–S) battery is considered one of the most promising technologies for next-generation energy storage. To realise its practical applications, electrodes with high areal sulfur loading, low-cost raw materials, and easily accessible fabrication processes are essential. Herein, we demonstrated the effectiveness of a commercially available black pigment, titanium black (TiB), as a multi-functional additive for sulfur electrodes. Benefiting from the amphipathic nature of TiB, it was easy to obtain a homogenous coating on a current collector (> 4 mg cm^{-2}) by applying a traditional slurry containing aqueous carboxymethyl cellulose/styrene-butadiene rubber as a binder. Contact angle measurements revealed much better electrolyte wettability for the electrode with the addition of TiB. Combined with a sparingly solvating electrolyte based on sulfolane and Li[N(SO$_2$CF$_3$)$_2$], the electrode showed excellent cycling performance and high Columbic efficiency at a relatively high current density. Finally, pouch cells were fabricated with low electrolyte/sulfur (E/S) ratio of 3.2 µL mg^{-1}, and a high energy density of 280 Wh kg^{-1} was achieved. Subsequent investigation of the gassing behaviour revealed that swelling of the charged cells at 60 °C was suppressed for half a month. This study may pave the way for designing Li–S batteries with practical utility.

1. Introduction

Rechargeable batteries with high energy densities and long cycle lives are urgently sought after due to the increasing demand for electric vehicles, hybrid electric vehicles, and large-scale power grids towards a sustainable society.[1–4] Conventional lithium-ion batteries based on Li-ion insertion chemistry have greatly contributed to these demands, but their energy density is approaching the theoretical limit (350 Wh kg^{-1}).[5,6] Therefore, they cannot necessarily satisfy further demands for higher energy densities. Elemental sulfur, an inexpensive, abundantly available material, has emerged as one of the most promising positive electrode active materials because of its high theoretical specific capacity (1672 mAh g^{-1}).[7,8] Nevertheless, the commercialisation of rechargeable Li–S batteries is still hindered by several important issues: the electronically insulating nature of sulfur and its discharge products (Li$_2$S$_x$, x = 1–8), the large volumetric expansion of 80% upon its full lithiation, and the dissolution and shuttle effects of lithium polysulfides (LiPS).[9–12] In addition, the excess amounts of electrolyte which are required to utilise the large specific capacity of sulfur severely reduce the energy density of the batteries.[13]

Significant progress has been made in improving the specific capacity, rate capability, and cycling performance of Li–S batteries using various strategies to solve the above-mentioned challenges.[14–16] For example, many advanced carbon materials with unique structures have been proposed as conductive matrices.[17,18] However, such carbon materials can only physically block LiPS diffusion because their non-polar surfaces have poor affinity for the polar LiPS. Hence, metal compounds with polar surfaces have been introduced to act as sulfur hosts and enhance the chemical interaction between LiPS and the substrates.[19-21] Unfortunately, most carbon and metal materials are fabricated via complex, high-cost processes. Besides, these materials are not suitable for practical applications due to the low capacities per total weight of the electrode materials and difficulties related to the slurry coating processes for the cathode.

Selection of the electrolyte is another critical factor because it greatly affects the energy density and rate capability of Li–S batteries. Thus far, electrolyte solutions consisting of Li[N(SO$_2$CF$_3$)$_2$] (Li[TFSA]) in mixtures of 1,3-dioxolane (DOL) and 1,2-dimethoxyethane (DME) have been widely used as liquid electrolytes.[22] However, these electrolyte solutions readily dissolve LiPS, which results in complicated dissolution/precipitation discharge/charge processes and poor capacity retention.[23] Elemental sulfur and the discharged products (Li$_2$S, Li$_2$S$_2$) are hardly soluble in the electrolyte, whereas the intermediate LiPS species (Li$_2$S$_x$, x = 4–8) are highly

a. Advanced Chemical Energy Research Centre, Institute of Advanced Sciences, Yokohama National University, 79-5 Tokiwadai, Hodogaya-ku, Yokohama 240-8501, Japan, E-mail: mwatanabe@ynu.ac.jp
b. Department of Chemistry and Life Science, Yokohama National University, 79-5 Tokiwadai, Hodogaya-ku, Yokohama 240-8501, Japan
† These two authors equally contributed to this work.

soluble. Therefore, the initial discharge process actually occurs in a catholyte (electrolyte with dissolved LiPS). Considering these facts, Li–S batteries using Li[TFSA] in DOL/DME as the electrolyte can only take advantage of the high discharge capacity of sulfur with excess electrolyte (electrolyte/sulfur (E/S) > 5), which can easily dissolve LiPS and results in a high-viscosity dissolved solution.[13,24,25] As a result, the energy density of the total battery system cannot be enhanced to the expected level. Additionally, the dissolved LiPS causes the shuttle effect and poor Coulombic efficiencies. LiNO$_3$ is frequently added to the electrolyte to react with the lithium anode and form a solid electrolyte interphase (SEI), which can block the shuttle effect.[21] However, LiNO$_3$ can be consumed at the anode during charge/discharge cycles and further cause gassing behaviour, as discussed later. Hence, some novel electrolyte solvents and additives need to be developed to further supress the LiPS dissolution and increase the sulfur utilization.[26,27]

We have proposed sparingly solvating electrolytes towards LiPS, which suppress the shuttle effect and enhance the cycle life and Coulombic efficiencies of Li–S batteries.[15,28] Solvate ionic liquids (SILs), typically consisting of Li[TFSA] and an equimolar amount of glyme (triglyme (G3) or tetraglyme (G4)), exhibit properties similar to those of conventional ionic liquids. In SILs, Li$^+$ and the glyme form a long-lived and robust 1:1 complex (solvate); therefore, the liquid actually consists of the solvate cation and the [TFSA]$^-$ anion with a negligible amount of free glyme.[29] Since LiPS species are ionic salts, coordination of the electrolyte to the cation (Li$^+$) or anion (PS$^-$) is essential for dissolution. Because the Lewis acidity of Li$^+$ is neutralised by the Lewis-basic glyme, the solvate cations have a low Lewis acidity. The Lewis basicity of the [TFSA]$^-$ anion itself is also exceptionally low. Therefore, the coordinating ability of the SIL to LiPS decreases, resulting in a poor LiPS solubility. This concept can be applied to other highly concentrated electrolyte solutions using sulfolane (SL), acetonitrile, etc.[25,28,30,31] However, these kinds of electrolytes also have several disadvantages, including poor wettabilities, high viscosities, and low ionic conductivities. To address these issues, we have also proposed co-solvent dilution by sparingly solvating solvents, such as 1,2,2-tetrafluoroethyl-2,2,3,3-tetrafluoropropyl ether (HFE), to lower the electrolyte viscosity, enhance the ionic conductivity, and further increase the electrolyte wettability.[15] It is worth mentioning that the electrolyte wettability also affects the electrode intrinsic properties, such as the porosity and compressed density, and thus, the battery performance.[32] A high-wettability sulfur cathode with low porosity could contribute to decreasing the E/S ratio of Li–S batteries. However, to the best of our knowledge, no studies have focused on improving the intrinsic wettability of sulfur cathodes.

Hence, as discussed above, although a large number of fundamental studies on Li–S battery materials have been reported, strategies towards practical Li–S batteries are, in stark contrast, quite lacking.[33,34] **Table S1** displays the requirements to achieve low-cost practical Li–S batteries with an energy density greater than 500 Wh kg^{-1}. Obviously, a high areal capacity of the sulfur cathode, low E/S ratio, and viable production methods using cheap and readily available materials are of great importance. Herein, we present a novel Li–S battery design using TiB as a cathode additive with low-cost raw materials, a simple electrode manufacturing process, and a sparingly solvating electrolyte. The addition of TiB enables a large-areal-capacity sulfur cathode by the simple application of a homogeneous slurry onto Al current collectors and improved the electrode wettability, which ensured high discharge capacity even at low E/S ratios. Furthermore, pouch-type Li–S batteries with high energy densities were successfully fabricated. We believe that our study affords a new perspective on future directions and prospects towards practical Li–S batteries.

2. Experimental

2.1 Preparation of Sulfur Cathodes

The sulfur/carbon composite cathode was prepared from a mixture of elemental sulfur (S$_8$, Wako Chemical, 75 wt%) and Ketjen Black (KB, ECP600JD, Lion Corporation, 25 wt%). KB and S$_8$ were mixed using an agitating mortar, then transferred to a vial and maintained at 155 °C for 12 h to allow for the diffusion of sulfur into the pores of KB. A typical slurry was made by mixing the S/KB composite, carboxymethyl cellulose (CMC, CMC2200, Daicel FineChem), and styrene-butadiene rubber (SBR, JSR Corporation) in distilled water at a weight ratio of 96.5:1.5:2. For comparison, 3 wt% TiB (Mitsubishi Material) was added to the slurry at a weight ratio of S/KB:TiB:CMC:SBR = 93.5:3:1.5:2. The obtained two kinds of slurry were both coated onto carbon-coated aluminium foils as current collectors and then dried in an oven at 60 °C for 12 h to obtain the cathodes Sulfur content for the TiB and TiB free electrodes is 70.1% and 72.3%, respectively. Then, the cathodes were cut into a disk shape (for coin cells) or rectangular shape (for pouch cells) and dried in an oven under vacuum at 40 °C for 12 h before use. The electrodes with and without TiB were denoted as the TiB electrode and TiB free electrode, respectively.

2.2 Preparation of Electrolytes

The SL-based highly concentrated electrolyte was prepared according to the method reported in our previous paper.[35] First, a highly concentrated [Li(SL)$_2$][TFSA] electrolyte was prepared by mixing SL (battery grade, Kishida Chemical) and Li[TFSA] (Solvay Japan, water content < 50 ppm) at a molar ratio of 2:1 to form a homogeneous solution. Then, HFE (Daikin Industries) was added to the above concentrated electrolyte to obtain a homogenous mixture of [Li(SL)$_2$][TFSA]-4HFE. The traditional electrolyte used in this study was composed of 1 M Li[TFSA] in DOL/DME (1/1 vol/vol) with 0.5 wt% LiNO$_3$ as an additive. All the mixing processes were carried out at room temperature in an Ar-filled glove box (VAC, dew point < −80 °C, [O$_2$] < 1 ppm).

2.3 Cell Assembly

A 2032 coin cell was assembled in an Ar-filled glove box using the sulfur cathode (14 mm in diameter), an Li metal anode (Honjo Metal, 16 mm in diameter), the electrolyte (80 μL), and a Celgard 3501 separator. For the pouch cells, a layer-by-layer

process was applied to laminate the cathodes (coating of either one or both sides of carbon coated Al current collector, 45×35 mm), separator, and anodes (50×40 mm). As the anode, Li metal coated on both sides of Cu foil (Li thickness = 90 μm, Honjo Metal) was used. The charge/discharge measurements (HJ1001SD8, Hokuto Denko) were performed at 30 °C with cut-off potentials of 1.0 and 3.3 V for the discharge and charge steps, respectively. The same type of coin cell made with the traditional DOL/DME electrolyte was subjected to charge/discharge measurements in the potential range 1.7–2.8 V. Galvanostatic intermittent titration technique (GITT) was used to demonstrate the polysulfide conversion in the electrode by using a potentiostat (VMP300, Bio-Logic). A 0.02 C constant current discharge was applied for 1 h and after that, the cell was left at open circuit potential for 2 h and the voltage equilibration is recorded.

2.4 Characterisation

To study the electrochemical products on the sulfur cathodes during cycling, the cells were disassembled in an Ar-filled glove box. The sulfur cathodes were separated and rinsed several times with pure HFE to remove the electrolyte residue. The pieces of the cathodes were all kept under an inert atmosphere during sample preparation and transfer to the testing instruments. Scanning electron microscopy (SEM) with energy-dispersive X-ray spectroscopy (EDX) was performed on a JEOL JSM-6390 to observe the morphologies of the electrodes and obtain elemental mappings. X-ray diffraction (XRD) measurements were performed using a Bruker D8 Advanced Diffractometer with Cu K$_\alpha$ radiation. X-ray photoelectron spectroscopy (XPS) measurements were performed on a Physical Electronics Quantera scanning X-ray microprobe. The XPS data were fitted using the Casa XPS software assuming a Gaussian/Lorentzian line shape after Shirley background correction. The contact angles of SL on the sulfur cathodes were measured using a Rame-Hart Model 190 contact angle goniometer at room temperature. A rheometer (Physica MCR301, Anton Paar) was used to measure the viscosity as a function of shear rate under dry air conditions at 30 °C using a cone and plate with a diameter of 25 mm and cone angle of 1°.

3. Results and Discussion

3.1 Fabrication of High-Sulfur-Loading Cathode

As shown in **Table S1**, the fabrication of high-sulfur-loading cathodes using feasible and low-cost materials is essential to obtain practical high-energy-density Li–S batteries. Although various advanced carbon and metal based materials have been studied, these materials are always obtained through special processes with high cost. **Fig. S1** shows sulfur cathodes cost calculated based on a typical practical 2 Ah pouch cell with various carbon/metal based hosts. It is apparent that specially treated hosts will make a significant increase in the cathode cost, especially when sulfur content is low in the electrode. As the sulfur content is further increased, the cost will decrease

correspondingly. Hence, host material and sulfur content in electrode are both the most critical parameters playing key role towards cathode cost reduction of Li-S battery. Considering this point, here, we chose KB as the carbon host, which is a commercially available nano-sized porous carbon material with a high specific surface area (1270 m^2 g^{-1}). However, this kinds of high-surface-area sulfur-host carbon materials without a unique design are highly difficult to fabricate into thick electrodes without cracks and pinholes.[36] Many attempts have been made to address these issues by modifying the binder structures and contents, introducing conductive polymers, or adopting self-assembly approaches.[37–39]

Considering the hydrophobic nature of the S/KB composite, we selected a high-polarity additive for the electrode. Titanium-based materials, including Ti$_4$O$_7$, TiO$_2$, TiO, and TiN, have been used as sulfur hosts as they show favourable electrochemical behaviours (**Table S2**). However, these materials are obtained through special processes, and most of these materials can hardly be produced in a large scale, which enhances the cathode cost, as shown in **Fig. S1**. Commercially available titanium-related materials that are easy to obtain have rarely been studied. Here, we employed a commercially available black pigment (TiB), which is non-toxic and cheap as an additive for the sulfur cathode slurry. The XRD pattern (**Fig. S2a**) suggests that the commercially available TiB is a mixture of TiN and TiO$_2$, and the SEM image (**Fig. S2b**) demonstrates that the morphology of TiB consists of well-distributed particles without any unusual morphology.

Nano-sized materials frequently require a large amount of polymer binder and conductive additive to construct a homogeneous and efficient electrode layer. To shed light on the effect of TiB, we exploited the traditional aqueous binder CMC/SBR at a content of 3.5 wt%. To ensure a high sulfur content in the cathode (> 70 wt%), no extra conductive carbon was added. **Fig. 1a** and **b** show the morphologies of the TiB free and TiB electrodes with a relative high areal sulfur loading (4 mg cm^{-2}) under low magnification, respectively. Many obvious cracks were observed on the TiB free electrode, possibly because the nano-sized S/KB particles can easily hold large amounts of water during the slurry mixing and coating process. During subsequent drying, the wet coating layer loses the water and shrinks to a much smaller volume,[36] resulting in the formation of numerous cracks. Therefore, a large amount of polymer binder is generally required to avoid crack formation. Impressively, the TiB electrode showed a homogenous coating without cracks on the current collector even though the sulfur loading was higher than 4 mg cm^{-2}.
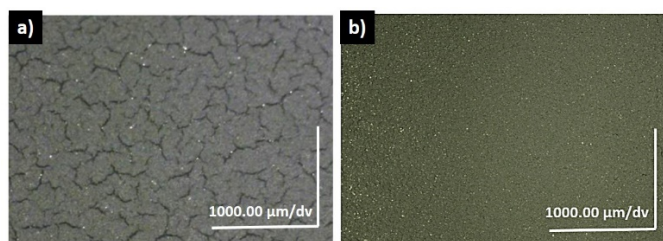
Fig. 1 SEM images under low magnification of the a) TiB free electrode (S loading < 4 mg cm^{-2}) and b) TiB electrode (S loading > 4 mg cm^{-2}).

To further assess the morphologies and elemental distribution, SEM and EDX analyses were conducted for the TiB free and TiB electrodes under higher magnification. As shown in **Fig. 2**, similar morphologies without any obviously aggregated particles were observed for both electrodes. The EDX elemental mappings of C and S further suggested a homogeneous distribution of the S/KB composite in both electrodes. For the TiB electrode, the Ti and N elemental mappings revealed well-dispersed TiB throughout the electrode, despite the use of a simple mixing process. To determine the stability of TiB during the slurry making process, the XRD pattern of the TiB electrode was compared with that of the pristine TiB material (**Fig. S3**). Besides the diffraction lines from the Al current collector, the strong signals could be assigned to crystalline S_8 and TiB. The signals ascribed to TiB indicate its high stability during the slurry making process.
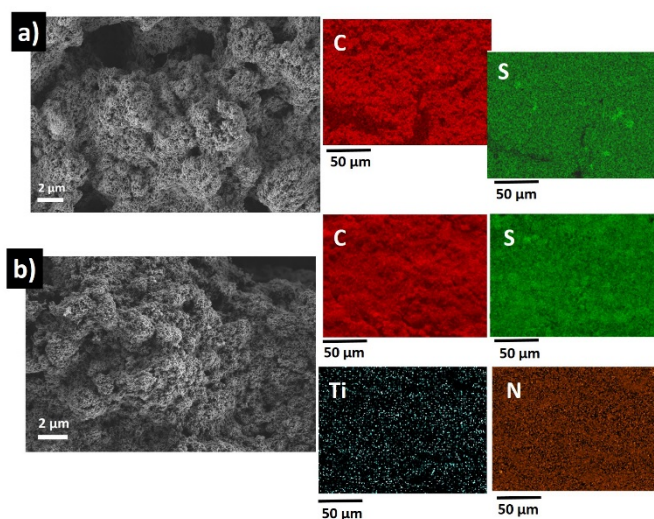
Fig. 2 SEM images and EDX elemental mappings of the a) TiB free electrode and b) TiB electrode.

It is believed that the physicochemical properties of slurries, which are influenced by interactions between the electroactive materials, conductive additives, and binders, play a key role in determining the electrode coating quality.[40] Hence, to understand the effect of TiB addition on the slurry properties, the rheological behaviour of the slurries with and without TiB was determined (**Fig. S4**). Consequently, an insight into the temporal stability of the electrode materials was gained from measurements of the rheological properties on the first day and

three days after preparation of the slurries. The slurries exhibited shear thinning behaviour, which is characterised by a decrease in viscosity with increasing applied shear rate. This behaviour results from the breaking of network structures originating from attractive interactions between the constituent materials of the slurries. On the first day, immediately after their preparation, both slurries showed reversible shear-thinning responses without hysteresis for a change in shear rate from 1 to 100 s^{-1}. However, in the case of the TiB free electrode slurry (**Fig. S4a**), a notable viscosity loss was observed after three days, whereas the viscosity of the TiB electrode slurry did not change significantly within the same period (**Fig. S4b**). Moreover, the TiB free electrode slurry showed a hysteresis behaviour, especially in the low shear rate region, with a slight increase in viscosity when the change in shear rate was reversed (decreased). The rheological properties of electrode slurries are dependent on the dispersion state of the constituent materials and their interactions. It has been reported that the aggregation of carbon materials with time causes an irreversible breakdown of the network structure.[41] Therefore, it is suggested that the viscosity loss of the TiB free electrode slurry after three days is due to disruption of the internal network structure. The slight increase in the viscosity of the three-day-old slurry during the reverse shear rate scan compared with that of the forward scan may originate from the breaking of carbon agglomerates at high shear rates and their consequent re-dispersing. The absence of such hysteresis in addition to the lack of change in viscosity with time for the TiB electrode slurry implies a relatively stable dispersion of S/KB in the presence of TiB.

3.2 Physicochemical Properties of the Electrodes

To investigate the interaction between TiB and the S/KB composite, XPS measurements were conducted. **Fig. 3a** displays the survey spectra of TiB and the TiB electrode, where the elemental S peak located at 167 eV is strong for the TiB electrode because of its high S content (> 70 wt%). Due to the surface sensitivity of the technique, the response from TiB in the electrode was analysed by high-resolution XPS. As shown in **Fig. 3b** (N 1s spectra), the peak at 397 eV indicated a Ti–N chemical interaction, and the appearance of a new peak at approximately 400 eV for the TiB electrode compared with the TiB free electrode indicated a strong N–S interaction between TiB and the S/KB composite.[36,42] For a further illustration, high-resolution S 2p and O 1s XPS of the TiB free and TiB electrodes was also performed. As shown in **Fig. 3c** and **d** (S 2p spectra of the TiB free and TiB electrodes, respectively), the main S 2p doublet at 164.3/165.5 eV is associated with S_8 molecules infused within the nano-channels of the KB host, which do not change with the introduction of the TiB additive.[43] New peaks corresponding to sulfate (SO_4^{2-}) and related species (S=O bonds) were also observed in the electrode spectra. Such species can be attributed to the oxidation of S, which may be caused by interactions between the O groups in the CMC binder and the S/KB composite.[43] In addition, compared with the TiB free electrode, the content of such sulfate species in the TiB electrode was much higher. It was previously reported that

nitrogen functional groups on carbon materials promote the formation of bonds between sulfur and oxygen functional groups.[44] Hence, in the TiB electrode, the existence of TiB further promotes the interaction between CMC and/or Ti–O and the S/KB composite, which results in higher sulfate content. The O 1s XP spectra also indicated S–O interactions between TiB and the S/KB composite, as discussed above for the S 2p spectra, with a peak corresponding to sulfates (S=O) (**Fig. 3e**, **f**) at 532 eV for both the TiB free and TiB electrode. Although it is challenging to discriminate S=O peaks from C=O peaks due to their large overlap, the TiB electrode showed a stronger S=O -signal than the TiB free electrode, which also indicates stronger S–O interactions. The above XPS results suggest that the simple mixing of TiB and the common S/KB composite in aqueous solvents in the presence of a small amount of CMC/SBR binder is effective to induce the strong binding of sulfur to TiB and/or CMC.
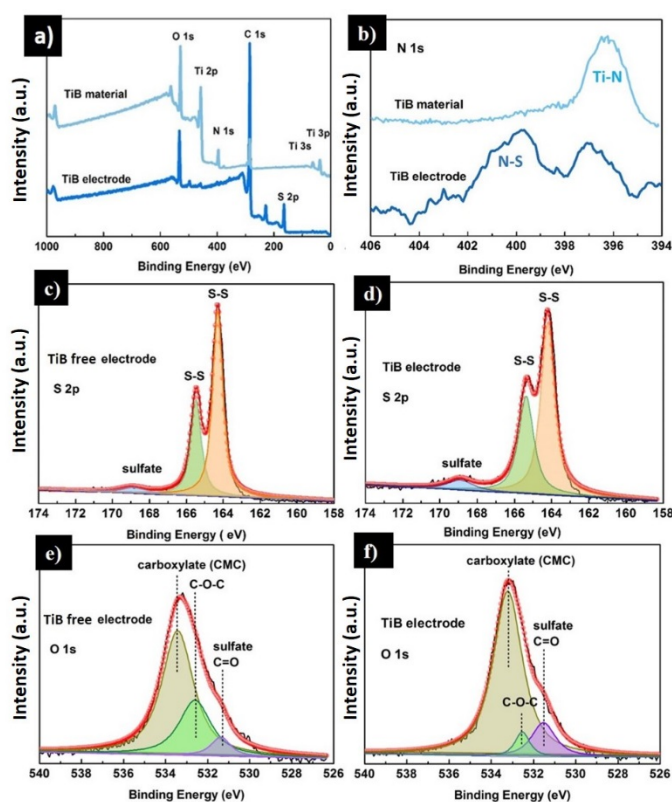

Fig. 3 a) XP survey spectra, b) N 1s spectra of the TiB material and TiB electrode, S 2p spectra of the c) TiB free and d) TiB electrodes, and O 1s spectra of the e) TiB free and f) TiB electrodes.

For high-energy-density Li–S batteries, the electrolyte wettability must be considered under lean electrolyte conditions (low E/S ratios). Especially, for thick sulfur cathodes, an improved wettability would guarantee sufficient ionic conduction pathways and the high utilisation of sulfur to maintain a high capacity. To explore whether the presence of the amphipathic TiB additive could improve the electrode wettability, we measured the contact angle of the electrolyte on the electrode surface. Instead of the commonly used water droplet, the SL solvent was dropped on the surface of the

electrodes for precise clarification of the wettability of the sparingly solvating electrolyte. The results of the static contact angle measurements on the electrodes (< 90° for a solvatophilic surface and > 90° for a solvatophobic surface) are shown in **Fig. 4a** and **b**. The much smaller contact angle on the TiB electrode surface revealed its solvatophilicity, which undoubtedly indicates better electrolyte wettability.
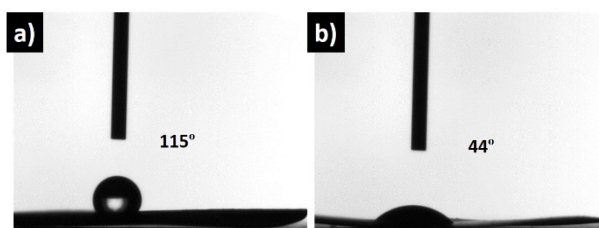

Fig. 4 Contact angle measurements using SL drops of the a) TiB free and b) TiB electrode surfaces.

3.3 Electrochemical Behaviour with Sparingly Solvating Electrolyte

The above physicochemical results suggested that the electrode with TiB as an additive has advantages over the TiB free electrode in terms of the coating quality and wettability. To evaluate its effect on the electrochemical behaviour, we first investigated the cycling performance of Li–S cells with a traditional electrolyte of 1 M Li[TFSA] in DOL/DME under a relatively high E/S ratio of 10. Although a good cycling performance can be achieved when a high amount of 5.0 wt% $LiNO_3$ is added to the traditional electrolyte,[45] only 0.5 wt% $LiNO_3$ was used in this study to investigate the intrinsic nature of the electrodes. All the cells were discharged at 0.021 C (1 C = 1672 mA g^{-1}) for the initial discharge to condition the electrodes with the electrolyte. As shown in **Fig. S5a**, two well-defined plateaus appeared in the voltage ranges 2.4–2.2 V and 2.2–1.8 V, corresponding to the conversion from S_8 to Li_2S_4 and from Li_2S_4 to Li_2S, respectively. Evidently, despite the higher sulfur loading, the TiB electrode showed a longer platform and delivered a higher capacity of 1160 mAh g^{-1} than that of the TiB free electrode, 1100 mAh g^{-1}. The subsequent cycling performance at 0.1 C (**Fig. S5b**) indicated that the cycling stability and Coulombic efficiency were significantly improved for the TiB electrode. After 80 cycles, a capacity of 700 mAh g^{-1} was retained for the TiB electrode, which can undoubtedly be ascribed to the strong affinity between TiB and the discharge products (LiPS). Conversely, the corresponding capacity for the TiB free electrode was only 300 mAh g^{-1}, along with rapidly declining Coulombic efficiencies, illustrating the severe shuttle effect of LiPS. It is interesting to note that an obvious capacity recovery was observed in the initial 20 cycles of the TiB free electrode, implying a gradually enhanced wettability.

Because of their insoluble features towards LiPS, sparingly solvating electrolytes can offer benefits for obtaining long cycles lives for Li–S cells. We have proposed Li[TFSA]-G4-HFE[15] and Li[TFSA]-SL-HFE[46] as sparingly solvating electrolytes for Li–S cells. These SL-based electrolytes showed lower LiPS solubilities

This journal is © The Royal Society of Chemistry 20xx

Energy Environ. Sci., 2020, **00**, 1-3 | **5**

and higher rate capabilities for Li–S cells compared with G4-based electrolytes.[46] The SL-based sparingly solvating electrolytes were also found to afford a significant improvement in Li-ion mass transfer, enabling faster solid-state sulfur redox reactions in high-performance Li–S cells.[46] Hence, the electrochemical performance of Li–S coin cells based on the sparingly solvating electrolyte [Li(SL)$_2$][TFSA]-4HFE with an E/S ratio of 6–7 was measured. As displayed in **Fig. 5a**, both the TiB free and TiB electrode showed high discharge capacities of nearly 1400 mAh g^{-1}. The subsequent cycling stability of the cells at 0.1 C is presented in **Fig. 5b**. After 200 cycles, the TiB electrode retained a capacity of 650 mAh g^{-1} for a retention of 73% relative to the first cycle at 0.1 C. In contrast, the TiB free electrode delivered a poor cycling stability, with a corresponding capacity and retention of 500 mAh g^{-1} and 60%,

Fig. 5 Electrochemical behaviour of Li–S coin cells with the sparingly solvating electrolyte [Li(SL)$_2$][TFSA]-4HFE: a) initial discharge curves of the TiB free and TiB electrodes at 0.021 C, b) cycling performance of the TiB free and TiB electrodes at 0.1 C, c) cycling performance of the TiB electrode at 0.2 C, and d) discharge curves of the TiB free and TiB electrodes at 60 °C and 0.021 C after discharging and charging to 100% SOC at 0.021 C and room temperature then being left under open-circuit conditions at 60 °C for 7 days.

respectively. Notably, the Coulombic efficiencies during cycling for both cells were almost 100%, indicative of suppression of the LiPS shuttle effect by the SL-based sparingly solvating electrolyte. Subsequently, the cells were investigated at higher current density. **Fig. 5c** displays the cycling stability at 0.2 C of a cell containing a TiB electrode with a higher sulfur loading of 4.5 mg cm^{-2}. After 100 cycles, the delivered capacity was higher than 500 mAh g^{-1}, with a nearly 100% Columbic efficiency. Unfortunately, the cell without TiB showed a discharge capacity of only 200 mAh g^{-1} (not shown here). Therefore, it is obvious that the cells assembled with the TiB electrode exhibit a high specific capacity, high rate capability, and long cycling life, which could be further ascribed to the improved wettability of the electrode and strong binding of sulfur to TiB. For comparison, the electrode with a higher TiB content (5 wt%, S/KB:TiB:CMC:SBR = 91.5:5:1.5:2) was also coated and evaluated in a coin cell. The initial several discharge curves with a relative high sulfur loading at 0.1 C were shown in **Fig. S6**. Obviously, higher content of TiB in the electrode gave a worse effect on the capacity delivery, which is undoubtedly ascribed to the decreased ionic conductivity of the electrode.
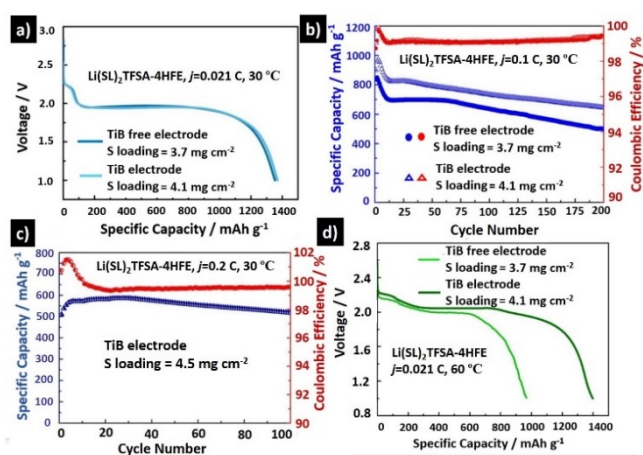
The self-discharge phenomenon in traditional DOL/DME-based electrolytes, which is mainly caused by the reactions of the lithium anode with LiPS diffusing from the cathode side, is one of the most serious issues which hinders the practical application of Li–S batteries.[47] Due to the suppressed solubility of LiPS in the [Li(SL)$_2$][TFSA]-4HFE electrolyte, the Li–S cells with the TiB free and TiB electrodes were first discharged and charged to 100% SOC at 0.021 C and left in open-circuit conditions at 60 °C for 7 days to accelerate the side reactions. **Fig. 5d** displays the subsequent discharge curves obtained at 60 °C and 0.021 C. Impressively, the cell with the TiB electrode maintained essentially the same capacity as it initially delivered at room temperature (**Fig. 5a**), indicating that negligible self-discharging occurred during storage. In addition, the higher discharge plateau at 60 °C (**Fig. 5d**) compared with that at room temperature (**Fig. 5a**) can undoubtedly be ascribed to the decreased viscosity of the electrolyte at elevated temperatures. On the other hand, the capacity of the cell with the TiB free electrode decreased to 1000 mAh g^{-1} due to self-discharge. This phenomenon can be attributed to the lessened LiPS dissolution in the TiB electrode cell at an elevated temperature, which may be due to the chemical binding between TiB and LiPS in the electrode.

3.4 Analysis of Electrodes after Electrochemical Tests

The underlying reason for the stable capacity of the TiB electrode was explored by examining the electrodes after cycling. The Li–S cells after 200 cycles (**Fig. 5b**) were disassembled and examined by SEM. **Fig. 6a** and **b** show the SEM images of the TiB free and TiB electrodes, respectively, in the charged state. A much more distinct porous nature without obvious cracks was observed for the TiB electrode even after extended cycling, which contrasts with the TiB free electrode and its severe cracks (indicated by red arrows). The discharged TiB free electrode (**Fig. 6c**) showed a dense region without any porosity on the surface (marked by a red circle). Consistent with the results of a previous study, electrochemically generated Li$_2$S, which has 180% of the volume of sulfur, efficiently fills the void space of the porous electrode.[48] This expansion and filling of void space significantly reduce the electrode porosity and lead to a dense coating layer.[45] For comparison, the SEM image of the discharged TiB electrode (**Fig. 6d**) illustrates that the

6 | *Energy Environ. Sci.*, 2020, **00**, 1-3

This journal is © The Royal Society of Chemistry 20xx

porosity could still be defined, indicating the homogeneous formation of Li_2S in the porous electrode structure. The enlarged images shown in **Fig. 6e** and **f** further demonstrate the morphological differences between the discharged TiB free and TiB electrodes. The SEM images (**Fig. 6d, f**) are consistent with those reported previously showing that the existence of a high-polarity host in the sulfur cathode could serve as the preferred seed for the subsequent formation of Li_2S and further redirect its growth.[49] In addition, due to the large volume change of sulfur during discharge/charge cycles, the formation of cracks is unavoidable in high-sulfur-loading electrodes with low binder content and no special design after long cycling periods. Hence, the SEM images of the TiB free electrode in the charged and discharged states both show the existence of large and numerous cracks. It is reasonable to consider that the filling of insulating Li_2S into the void space of the porous TiB free electrode and the formation of many large cracks led to its poor cycling performance and greatly reduced discharge capacity. Oppositely, due to the high coating quality brought via the strong interactions between the polarity TiB additive and KB/S composite, TiB electrode showed much better morphology retention even after extended cycling life.
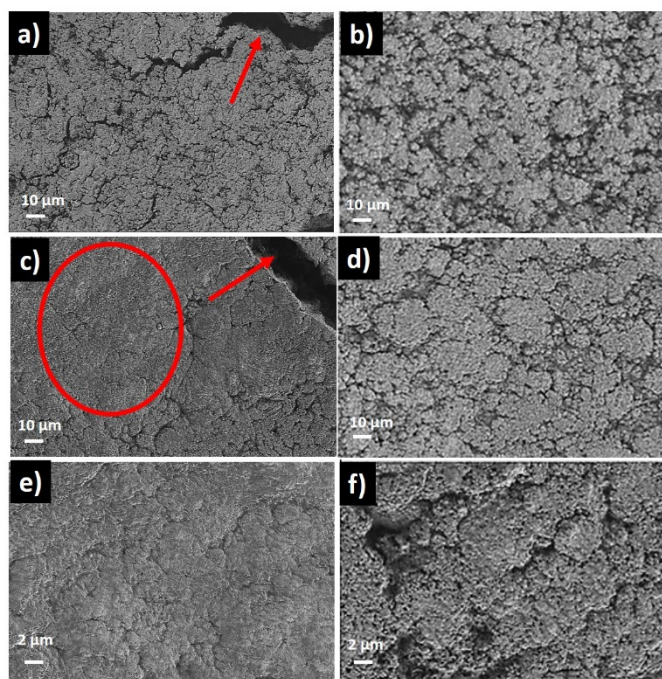
Fig. 6 SEM images of the electrodes after 200 cycles at 0.1 C (**Fig. 5b**): a), b) charged state and c), d) discharged state of the TiB free and TiB electrodes, respectively, with e), f) enlarged discharged state images.

To further demonstrate the species generated in the electrodes during the discharge/charge cycles, we conducted XPS measurements of the TiB free and TiB electrodes in the charged state after 200 cycles (**Fig. 5b**). As shown in the survey spectra in **Fig. S7a** and **c**, a trace Ti 2p signal and more distinct N 1s signal were observed for the TiB electrode compared with the TiB free electrode, which can be attributed to the presence of the TiB

additive. **Fig. S7b** and **d** show the high-resolution S 2p XP spectra of the TiB free and TiB electrodes, respectively. The SO_3 (169 eV) and SO_2/NSO_2 (167.2 eV) signals which overlap may originate from SL and Li[TFSA] decomposition.[50,51] Notably, besides the C–S peak, the spectrum of the TiB free electrode indicated the presence of unconverted Li_2S (S 2p doublet at 160.4/161.6 eV). In contrast, a stronger C–S peak and no Li_2S signal were observed for the charged TiB electrode, indicating the full oxidation of Li_2S. Considering the surface sensitivity of XPS, these results provide conclusive evidence for the incomplete reaction of Li_2S in the charged TiB free electrode. As was also confirmed by the SEM image in **Fig. 6c**, the dense and insulating Li_2S filling the void space of the porous electrode via volume expansion would lead to structural deterioration, which further decreases its conversion to sulfur.[52] On the other hand, in the TiB electrode, the transition of Li_2S to sulfur during the prolonged cycling process was accelerated by the presence of TiB. The further GITT experiments (**Fig.S8**) also clearly showed the difference during discharge process for the TiB and TiB free electrodes. At the beginning of discharge, the difference is not so obvious. However, at the capacity higher than 800 mAh g^{-1}, the equilibrium potential for the TiB electrode is higher and the polarization is smaller than that for the TiB-free electrode, which indicates the interaction between TiB and LiPS and facilitation of the conversion of LiPS to Li_2S.[53,54] It was reported that the TiO_2–TiN heterostructure as an S matrix can promote the fast conversion of LiPS into insoluble products.[55] Hence, our results is consistent with the previous results.

3.5 High-Energy-Density Pouch Cells

Although significant progress has been made in terms of coin cell studies, a significant gap remains between coin cells and practical pouch cells.[56] Hence, the fabrication of pouch cells is essential to achieve high-energy-density Li–S cells and to investigate the electrode stability and electrochemical properties under extremely lean electrolyte conditions (low E/S).

First, in order to study how the volume energy density is altered by the thickness of cathode, thickness of the TiB free and TiB electrodes with various S loading is studied. As displayed in **Fig. S9(a)**, obviously, TiB free electrodes show dramatical thickness increases when the sulfur loading is higher than 4 mg cm^{-2}. In contrast, due to the uniformly distributed KB/S composite, the thickness the TiB electrodes is thinner than that of the TiB free electrodes, and its increase with S loading is moderate. Further calculation of volume energy density based on the practical 2 Ah Li–S pouch cell with sulfur loading of 5 mg cm^{-2} was also conducted. The upper and lower plots in **Fig. S9(b)** corresponds to volume energy density calculated from the TiB free and TiB electrode thickness, respectively, under several sulfur utilizations. It is clearly demonstrated that with higher sulfur utilization, the cells show a larger variation range of the volume energy densities. Typically, the TiB electrode shows volume energy density of as high as 850 Wh L^{-1} under the sulfur utilization of 1200 mAh g^{-1} due to its lower electrode thickness, however, the corresponding value for the TiB free electrode is only 650 Wh L^{-1}.

This journal is © The Royal Society of Chemistry 20xx

Energy Environ. Sci., 2020, **00**, 1-3 | **7**

Second, for the specific energy density of practical Li-S battery, the electrolyte to sulfur ratio is the critical parameters. The most important factor in determining the necessary amount of electrolyte is the cathode porosity. Especially, the tap density of sulfur cathodes is much lower than that of transition metal oxide lithium-ion battery cathodes, which is one of the reasons why lean electrolyte conditions in Li–S cells are difficult. Therefore, to achieve lean electrolyte conditions, it is essential to increase the tap density, i.e., decrease the cathode porosity. To evaluate the effect of TiB on the tap density of the electrodes, TiB free and TiB electrodes with different compression ratios (85%, 75%, and 65% electrode thickness relative to the initial thickness) were prepared. The corresponding discharge capacities at 0.021 C were measured using coin cells. As shown in **Fig. 7**, up to a compression ratio of 85%, the capacity delivered from the electrodes did not greatly change, remaining higher than 1200 mAh g^{-1}. Upon increasing the compression ratio to 75%, a larger capacity reduction occurred for the TiB free electrode. Impressively, the TiB electrode still delivered a high capacity of 1100 mAh g^{-1} at the much higher compression ratio of 65%, whereas the corresponding value for the TiB free electrode was lower than 800 mAh g^{-1}. The discharge curves obtained at the different compression ratios displayed in **Fig. S10** clearly show the higher discharge voltage and plateau capacity of the TiB electrode than the TiB free one. Electrodes with high compression ratios may block the continuous electrolyte diffusion pathways, under which conditions the electrolyte wettability should become a significant issue. As illustrated by **Fig. 4**, the improved electrolyte wettability from the TiB additive would supply sufficient ionic conduction pathways and result in the higher utilisation of sulfur in the cathode, even under high compression.
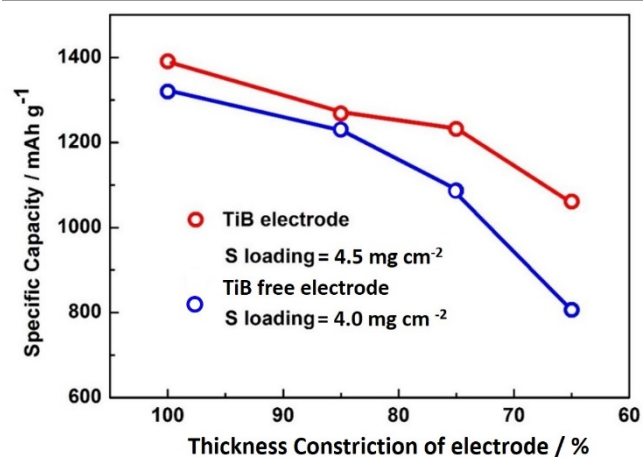

Fig. 7 Specific capacities at 0.021 C of the TiB free and TiB electrodes with different compression ratios relative to the initial thickness. The electrolyte was [Li(SL)$_2$][TFSA]-4HFE at E/S = 6–7.

Since the reduced porosity of the TiB electrode via compression still affords a high discharge capacity, we fabricated pouch cells to further reduce the E/S ratios through a layer-by-layer strategy using four cathode pieces and three anode pieces (**Fig. S11**). A thickness constriction ratio of 85% was explored for the

TiB and TiB free electrodes, and the [Li(SL)$_2$][TFSA]-4HFE electrolyte was used at E/S = 3.2. As shown by the discharge curves at 0.1 C in **Fig. 8**, the cell with the TiB electrodes showed a capacity of nearly 1300 mAh g^{-1} with a higher discharge potential, whereas the TiB free electrode cell displayed a corresponding value of 1100 mAh g^{-1}. A relatively high energy density of 280 Wh kg^{-1} was realised by the cell with the TiB electrodes (calculated based on the theoretical consumption of lithium and without the Al laminate film weight). For comparison, the TiB free electrode using 1 M Li[TFSA] in DOL/DME electrolyte with the same E/S value was also measured, but the cell exhibited a very poor capacity. This result is consistent with a previous work suggesting that E/S > 5 is necessary to attain a high discharge capacity for DOL/DME electrolyte cells.[57]

At a fixed E/S ratio, as the total amount of sulfur in the pouch cell increases, the energy density will also increase. Considering previous calculations,[34] we further calculated the energy density of a practical 2 Ah Li–S pouch cell. Of the involved components, the masses of the sulfur areal loading, tab, and Al package film were fixed, while that of the other components such as the binder, TiB additive, lithium anode, and electrolyte changed with the number of laminating layers (see the details in **Table S4**). Clearly, an energy density of 300 Wh kg^{-1} would no longer be a bottleneck restricting the actual energy density.
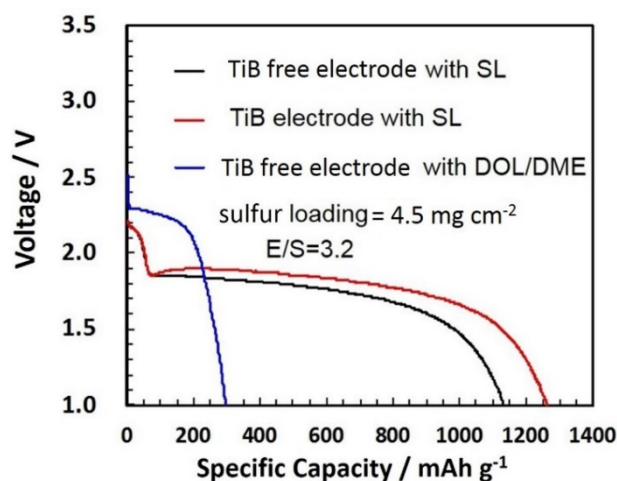

Fig. 8 First discharge curves at 0.1 C of pouch cells using the TiB free and TiB cathodes with a constriction ratio of 85%. The electrolytes were either conventional DOL/DME or the sparingly solvating electrolyte [Li(SL)$_2$][TFSA]-4HFE.

For a further comparison of the cycling performance, pouch cells using either the DOL/DME electrolyte or the sparingly solvating electrolyte with an E/S ratio of 5.5 were also fabricated. **Fig. S12a** shows the discharge curves of the TiB free electrode with the DOL/DME electrolyte at 0.1 C. As expected, due to the increased amount of electrolyte (E/S = 5.5) compared with cells corresponding to the results in **Fig. 8** (E/S = 3.2), the cell delivered an initial discharge capacity of 1100 mAh g^{-1} with two well-defined plateaus in the voltage ranges 2.4–2.2 and 2.2–1.8 V. The higher charging capacities compared with the corresponding discharging capacities indicated the severe

8 | *Energy Environ. Sci.*, 2020, **00**, 1-3

This journal is © The Royal Society of Chemistry 20xx

dissolution of LiPS in the electrolyte. In addition, the capacity fading with cycling was serious, and unstable charging behaviour was observed as early as the 10th cycle, possibly due to lithium dendrite formation, which would accompany severe side reactions on the lithium metal with highly dissolved LiPS by the shuttle effect. A further comparison of the cycling performance with the sparingly solvating electrolyte cells is shown in **Fig. S12b**. Clearly, the TiB electrode cell showed a more stable cycling performance than the TiB free electrode cell. After 30 cycles, the discharge capacity of the TiB electrode cell remained above 1000 mAh g^{-1}, whereas severe degradation occurred in the TiB free electrode cell after 20 cycles. Under the high sulfur loading and lean electrolyte conditions of the pouch cells, the improved electrolyte wettability of the TiB electrode would preserve more electrolyte for the anode during subsequent cycling, which results in a much more stable cycling performance than that of the TiB free electrode cell.
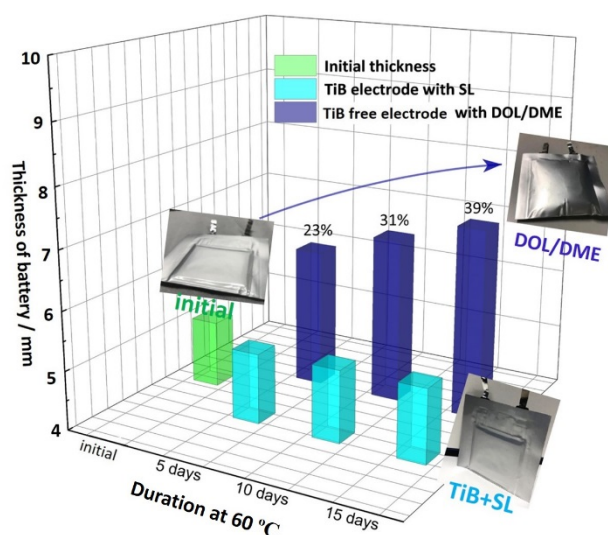
To further probe the SEI of the lithium anode, we disassembled the pouch cells with the TiB and TiB free electrodes using the sparingly solvating electrolyte after the experiments corresponding to **Fig. S12b**. To exclude the effect of the electrolyte, all the electrodes were first etched for 10 s with an argon beam. The high-resolution F 1s XP spectra (**Fig. S13a**, **b**) showed signals at 685.7 and 688.4 eV assignable to F–Li and F–C, respectively, suggesting that the F element in the SEI layer was present in both inorganic (F–Li) and organic (F–C) forms. In addition, the intensity of the Li–F peak was significantly higher for the SEI layer formed in the TiB electrode pouch cell. The Li 1s XP spectra (**Fig. S13c**) also displayed stronger signals corresponding to Li–F and Li–O for the TiB electrode cell. The measured atomic compositions of the lithium anode surfaces are given in **Table S5**. It is clear that the SEI in the TiB electrode cell contained greater F, Li, and O contents and a lower C content than the TiB free electrode cell, indicating that the SEI of the former was more inorganic than that of the latter. At a low E/S value, the cathode with a higher wettability would require a minimal amount of the electrolyte to promote smooth and homogeneous cathode reactions, which in turn would also ensure smooth and homogeneous anode reactions with sufficient electrolyte at the anode interface. Hence, these XPS results indicate that a stable, inorganic-rich SEI layer was formed in the TiB electrode pouch cell, which might be attributable to sufficient electrolyte at the anode interface. The SEM images shown in **Fig. S14** further illustrate the evolution of the cathode morphologies. Compared with the coin cell (**Fig. 6c**), a much denser Li_2S layer with severe cracks was observed for the pouch cell with the TiB free electrode. It has been shown that Li_2S precipitation is dependent on current density, where a high current density leads to the formation of a thick Li_2S layer.[58] The high porosity and uniform morphology of the TiB electrode further evidence its role in redirecting the growth pathway of Li_2S even at a relatively high discharge rate.

3.6 Gassing Behaviour of Pouch Cells

Although $LiNO_3$ has been considered an effective additive for the protection of lithium anodes, cells containing $LiNO_3$ may produce gases and swell above 40 °C, which would render them impractical.[33,59,60] Hence, a pouch cell with conventional DOL/DME and the TiB free electrode and a pouch cell with the sparingly solvating electrolyte and TiB electrode were charged to 100% SOC after initial 5 cycles, then placed in an oven at 60 °C. The gassing degrees within different durations were determined according to the change in the cell thickness. As shown in **Fig. 9**, compared with the freshly fabricated cell, no obvious thickness change was observed for the cell with the sparingly solvating electrolyte, even for an expended duration of half a month. In contrast, the corresponding swelling degree for the cell with the DOL/DME electrolyte reached nearly 40%. These results clearly demonstrate that the combined use of the TiB electrode and sparingly solvating electrolyte will pave a new way for designing Li–S batteries with practical utility.

Fig. 9 Swelling change of charged pouch cells for different durations at 60 °C.

4. Conclusion

This journal is © The Royal Society of Chemistry 20xx

Energy Environ. Sci., 2020, **00**, 1-3 | **9**

In summary, herein we have proposed a novel design for high-energy-density Li–S batteries aiming at their practical application. We focused on low-cost starting materials, a multi-functional additive for the sulfur electrode, a simple electrode manufacturing process, and a sparingly solvating electrolyte. Commercially available KB without any special design or treatment served as the carbon host. We first explored commercially available TiB as an additive for the electrode. With the aid of the affinity of TiB towards sulfur, it was possible to prepare a thick and homogenous coating on a current collector (> 4 mg cm^{-2}) using a traditional aqueous slurry with CMC/SBR as a binder. Meanwhile, the wettability of the thick electrode towards the electrolyte was also improved by the highly solvatophilic nature of the TiB material, even with a viscous and sparingly solvating electrolyte. Finally, a pouch cell with an extremely low E/S value of 3.2 was successfully fabricated, which exhibited a high energy density of 280 Wh kg^{-1}. We believe that our work affords a new perspective on the design of practical Li–S batteries and represents great prospects for their future applications.

Conflicts of interest

There are no conflicts to declare.

Acknowledgements

References

1 J. B. Goodenough, *Acc. Chem. Res*., 2013, **46**, 1053.
2 B. Dunn, H. Kamath and J. M. Tarascon, *Science*, 2011, **334**, 928.
3 J. M. Tarascon, *Philos. Trans. R. Soc., A*, 2010, **368**, 3227.
4 D. Larcher and J. M. Tarascon, *Nat. Chem*., 2015, **7**, 19.
5 J. B. Goodenough and K. S. Park, *J. Am. Chem. Soc*., 2013, **135**, 1167.
6 N. S. Choi, Z. H. Chen, S. A. Freunberger, X. L. Ji, Y. K. Sun, K. Amine, G. Yushin, L. F. Nazar, J. Cho and P. G. Bruce, *Angew. Chem. Int. Ed*., 2012, **51**, 9994.
7 A. Manthiram, Y. Fu, S. H. Chung, C. Zu and Y. S. Su, *Chem. Rev*., 2014, **114**, 11751.
8 P. G. Bruce, S. A. Freunberger, L. J. Hardwick and J. M. Tarascon, *Nat. Mater*., 2012, **11**, 19.
9 D. Bresser, S. Passerini and B. Scrosati, *Chem. Commun*., 2013, **49**, 10545.
10 A. Manthiram, Y. Fu and Y. S. Su, *Acc. Chem. Res*., 2012, **46**, 1125.
11 W. J. Chung, J. J. Griebel, E. T. Kim, H. Yoon, A. G. Simmonds, H. J. Ji, P. T. Dirlam, R. S. Glass, J. J. Wie, N. A. Nguyen, B. W. Guralnick, J. J. Park, A. Somogyi, P. Theato, M. E. Mackay, Y. E. Sung, K. Char and J. Pyun, *Nat. Chem*., 2013, **5**, 518.
12 X. Ji and L. F. Nazar, *J. Mater. Chem*., 2010, **20**, 9821.
13 F. Y. Fan and Y. M. Chiang, *J. Electrochem. Soc*., 2017, **164**, A917.
14 C. J. Hart, M. Cuisinier, X. Liang, D. Kundu, A. Garsuch and L. F. Nazar, *Chem. Commun*., 2015, **51**, 2308.
15 K. Dokko, N. Tachikawa, K. Yamauchi, M. Tsuchiya, A. Yamazaki, E. Takashima, J. W. Park, K. Ueno, S. Seki, N. Serizawa and M. Watanabe, *J. Electrochem. Soc*. 2013, **160**, A1304.
16 X. L. Ji, K. T. Lee and L. F. Nazar, *Nat. Mater*., 2009, **8**, 500.
17 Z. Li, J. T. Zhang, B. Y. Guan, D. Wang, L. M. Liu and X. W. (D.) Lou, *Nat. Commun*., 2016, **7**, 13065.
18 M. S. Balogun, C. Li, Y. Zeng, M. Yu, Q. Wu, M. Wu, X. Lu and Y. Tong, *J. Power Sources*, 2014, **272**, 946.
19 Q. J. Shao, P. F. Lu, L. Xu, D. C. Guo, J. Gao, Z. S. Wu, J. Chen, *J. Energy Chem*., 2020, **51**, 262.
20 Z. Xiao, Z. Yang, L. Wang, H. Nie, M. Zhong, Q. Lai, X. Xu, L. Zhang and S. Huang, *Adv. Mater*., 2015, **27**, 2891.
21 W. Kong, L. Yan, Y. Luo, D. Wang, K. Jiang, Q. Li, S. Fan and J. Wang, *Adv. Funct. Mater*., 2017, **27**, 1606663.
22 C. Barchasz, J. C. Lepretre, S. Patoux and F. Alloin, *J. Electrochem. Soc*., 2013, **160**, A430.
23 R. Xu, I. Belharouak, J. C. M. Li, X. F. Zhang, I. Bloom and J. Bareño, *Adv. Energy Mater*., 2013, **3**, 833.
24 G. Li, S. Wang, Y. Zhang, M. Li, Z. Chen and J. Lu, *Adv. Mater*., 2018, **30**, 1705590.
25 G. Zhang , H. J. Peng, C. Z. Zhao, X. Chen, L. D. Zhao, P. Li, J. Q. Huang, Q. Zhang, *Angew. Chem. Int. Ed*., 2018, **57**, 16732.
26 M. Zhao, B. Q. Li, X. Chen, J. Xie, H. Yuan, J. Q. Huang, *Chem*., 2020, **6**, 3297.
27 M. Cuisinier, P. E. Cabelguen, B.D. Adams, A. Garsuch, M. Balasubramanian and L. F. Nazar, *Energy Environ. Sci*., 2014, **7**, 2697.
28 S. Zhang, K. Ueno, K. Dokko and M. Watanabe, *Adv. Energy Mater*., 2015, **5**, 1500117.
29 N. Tachikawa, K. Yamauchi, E. Takashima, J. W. Park, K. Dokko and M. Watanabe, *Chem. Commun*., 2011, **47**, 8157.
30 J. Zheng, G. Ji, X. Fan, J. Chen, Q. Li, H. Wang, Y. Yang, K. C. DeMella, S. R. Raghavan and C. Wang, *Adv. Energy Mater*., 2019, **9**, 1803774.
31 Y. Yamada, K. Furukawa, K. Sodeyama, K. Kikuchi, M. Yaegashi, Y. Tateyama and A. Yamada, *J. Am. Chem. Soc*., 2014, **136**, 5039.
32 S. G. Lee and D. H. Jeon, *J. Power Sources*, 2014, **265**, 363.
33 T. Cleaver, P. Kovacik, M. Marinescu, T. Zhang and G. Offer, *J. Electrochem. Soc*., 2018, **165**, A6029.
34 M. Zhao, B. Q. Li, H. J. Peng, H. Yuan, J. Y. Wei and J. Q. Huang, *Angew. Chem. Int. Ed*., 2020, **59**, 12636.
35 T. Seita, Y. Matsumae, J. Liu, R. Tatara, K. Ueno, K. Dokko and M. Watanabe, *ACS Energy Lett*., 2020, **5**, 1.
36 D. P. Lv, J. M. Zheng, Q. Y. Li, X. Xie, S. Ferrara, Z. M. Nie, L. B. Mehdi, N. D. Browning, J. G. Zhang, G. L. Graff, J. Liu and J. Xiao, *Adv. Energy Mater*., 2015, **5**, 1402290.
37 H. S. Sohn, M. L. Gordin, T. Xu, S. R. Chen, D. P. Lv, J. X. Song, A. Manivannan and D. H. Wang, *ACS Appl. Mater. Interfaces*, 2014, **6**, 7596.
38 T. Xu, J. Song, M. L. Gordin, H. Sohn, Z. Yu, S. Chen and D. Wang, *ACS Appl. Mater. Interfaces*, 2013, **5**, 11355.
39 W. Chen, T. Qian, J. Xiong, N. Xu, X. J. Liu, J. Liu, J. Q. Zhou, X.W. Shen, T. Z. Yang, Y. Chen and C. L. Yan, *Adv. Mater*., 2017, **29**, 1605160.
40 J. R. Owen, *Chem. Soc. Rev*., 1997, **26**, 259.
41 K. Y. Cho, Y. I. Kwon, J. R. Youn and Y. S. Song, *Mater. Res. Bull*., 2013, **48**, 2922.
42 Z. Cui, C. Zu, W. Zhou, A. Manthiram and J. B. Goodenough, *Adv. Mater*., 2016, **28**, 6926.
43 P. Bhattacharya, M. I. Nandasiri, D. P. Lv, A. M. Schwarz, J. T. Darsell, W. A. Henderson, D. A. Tomalia, J. Liu, J. G. Zhang and J. Xiao, *Nano Energy*, 2016, **19**, 176.
44 J. Song, T. Xu, M. L. Gordin, P. Zhu, D. Lv, T. B. Jiang, Y. Chen, Y. Duan and D. Wang, *Adv. Funct. Mate*r., 2014, **24**, 1243.

10 | *Energy Environ. Sci.*, 2020, **00**, 1-3

This journal is © The Royal Society of Chemistry 20xx

45 W. Li, H. Yao, K. Yan, G. Zheng, Z. Liang, Y. M. Chiang and Y. Cui, *Nat. Commun*., 2015, **6**, 7436.
46 A. Nakanishi, K. Ueno, D. Watanabe, Y. Ugata, Y. Matsumae, J. L. Liu, M. L. Thomas, K. Dokko and M. Watanabe, *J. Phys. Chem. C*, 2019, **123**, 14229.
47 N. Azimi, Z. Xue, N. D. Rago, C. Takoudis, M. L. Gordin, J. X. Song, D. H. Wang and Z. C. Zhang, *J. Electrochem. Soc.*, 2015, **162**, A64.
48 H. Chu, H. Noh, Y. J. Kim, S. Yuk, J. H. Lee, J. Lee, H. Kwack, Y. Kim, D. K. Yang and H. T. Kim, *Nat. Commun.*, 2019, **10**, 188, https://doi.org/10.1038/s41467-018-07975-4
49 Z. L. Xu, S. J. Kim, D. H. Chang, K. Y. Park, K. S. Dae, K. P. Dao, J. M. Yuk and K. Kang, *Energy Environ. Sci.*, 2019, **12**, 3144.
50 J. Alvarado, M. A. Schroeder, M. Zhang, O. Borodin, E. Gobrogge, M. Olguin, M. S. Ding, M. Gobet, S. Greenbaum, Y. S. Meng and K. Xu, *Mater. Today*, 2018, **21**, 341.
51 Q. Zhang, J. J. Chen, X. Y. Wang, C. Yang, M. S. Zheng and Q. F. Dong, *Phys. Chem. Chem. Phys.*, 2015, **17**, 10353.
52 J. H. Yan, X. B. Liu and B. Y. Li, *Adv. Sci.*, 2016, **3**, 1600101.
53 C. W. Lee, Q. Pang, Q. Pang, S. Ha, L. Cheng, S. D. Han, K. R. Zavadil, K. G. Gallagher, L. F. Nazar, M. Balasubramanian *ACS Cent. Sci.*, 2017, **3**, 605.
54 C. Weller, J. Pampel, S. Dörfler, H. Althues, S. Kaskel, *Energy Technol.,* 2019, **7**, 1900625.
55 T. H. Zhou, W. Lv, J. Li, G. M. Zhou, Y. Zhao, S. X. Fan, B. L. Liu, B. H. Li, F. Y. Kang and Q. H. Yang, *Energy Environ. Sci*., 2017, **10**, 1694.
56 B. Cheng, C. Yan, J. Q. Huang, P. Li, L. Zhu, L. Zhao, Y. Y. Zhang, W. C. Zhu, S. T. Yang and Q. Zhang, *Energy Storage Mater.*, 2017, **6**, 18.
57 M. Hagen, P. Fanz and J. Tubke, *J. Power Sources*, 2014, **264**, 30.
58 L. Kong, J. X. Chen, H. J. Peng, J. Q. Huang, W. C. Zhu, Q. Jin, B. Q. Li, X. T. Zhang and Q. Zhang, *Energy Environ. Sci*., 2019, **12**, 2976.
59 C. Qu, Y. Chen, X. Yang, H. Zhang, X. Li and H. Zhang, *Nano Energy*, 2017, **39**, 262.
60 C. Weller, S. Thieme, P. Härtel, H. Althues, S. Kaskel, *J. Electrochem. Soc.*, 2017, 164, A3766.

This journal is © The Royal Society of Chemistry 20xx

Energy Environ. Sci., 2020, **00**, 1-3 | **11**